**iScience, Volume *23***

## Supplemental Information

# Targeting SMYD3 to Sensitize Homologous Recombination-Proficient Tumors to PARP-Mediated Synthetic Lethality

**Paola Sanese, Candida Fasano, Giacomo Buscemi, Cinzia Bottino, Silvia Corbetta, Edoardo Fabini, Valentina Silvestri, Virginia Valentini, Vittoria Disciglio, Giovanna Forte, Martina Lepore Signorile, Katia De Marco, Stefania Bertora, Valentina Grossi, Ummu Guven, Natale Porta, Valeria Di Maio, Elisabetta Manoni, Gianluigi Giannelli, Manuela Bartolini, Alberto Del Rio, Giuseppina Caretti, Laura Ottini, and Cristiano Simone**

| Compound | Amino acid sequence | Molecular weight (Da) |
|---|---|---|
| P1 | NFF | 440,5 |
| P2 | DFF | 441,5 |
| P3 | LFF | 439,6 |
| P4 | FFF | 473,6 |
| P5 | QFF | 454,5 |
| P6 | KFF | 454,6 |
| P7 | NIF | 406,5 |
| P8 | NYF | 456,5 |
| P9 | NAF | 364,4 |
| P10 | NDF | 408,4 |
| P11 | NHF | 430,5 |
| P12 | NNF | 407,4 |
| P13 | NFI | 406,5 |
| P14 | NFY | 456,5 |
| P15 | NFA | 364,5 |
| P16 | NFH | 430,5 |
| P17 | NFW | 479,5 |
| P18 | NFR | 449,5 |
| P19 | NFK | 421,5 |

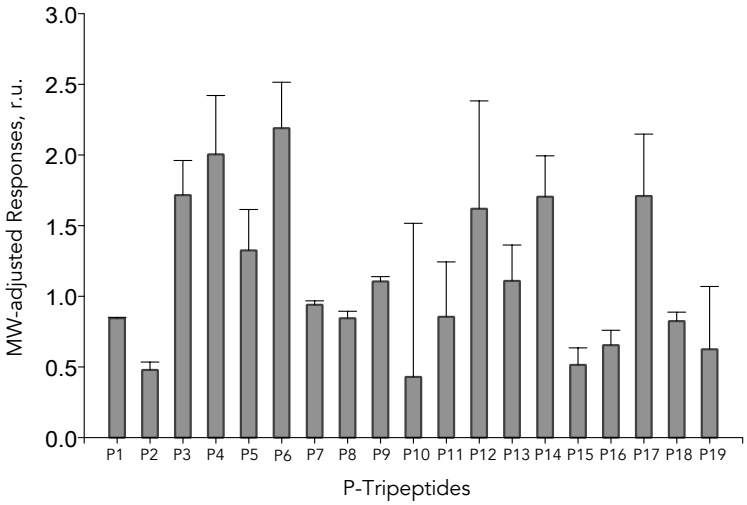


**Figure S1. SPR analysis of selected P-tripeptides interaction with SMYD3, (Related to Figure 1).**
Left: List of P-tripeptides with their amino acid composition and molecular weight. Right: Histogram of MW-adjusted SPR responses for the tested P-tripeptides. Shown double-referenced responses refer to the SAM-free assay. No difference in binding responses between SAM-free and SAM-saturated binding events emerged, suggesting no allosteric effect.

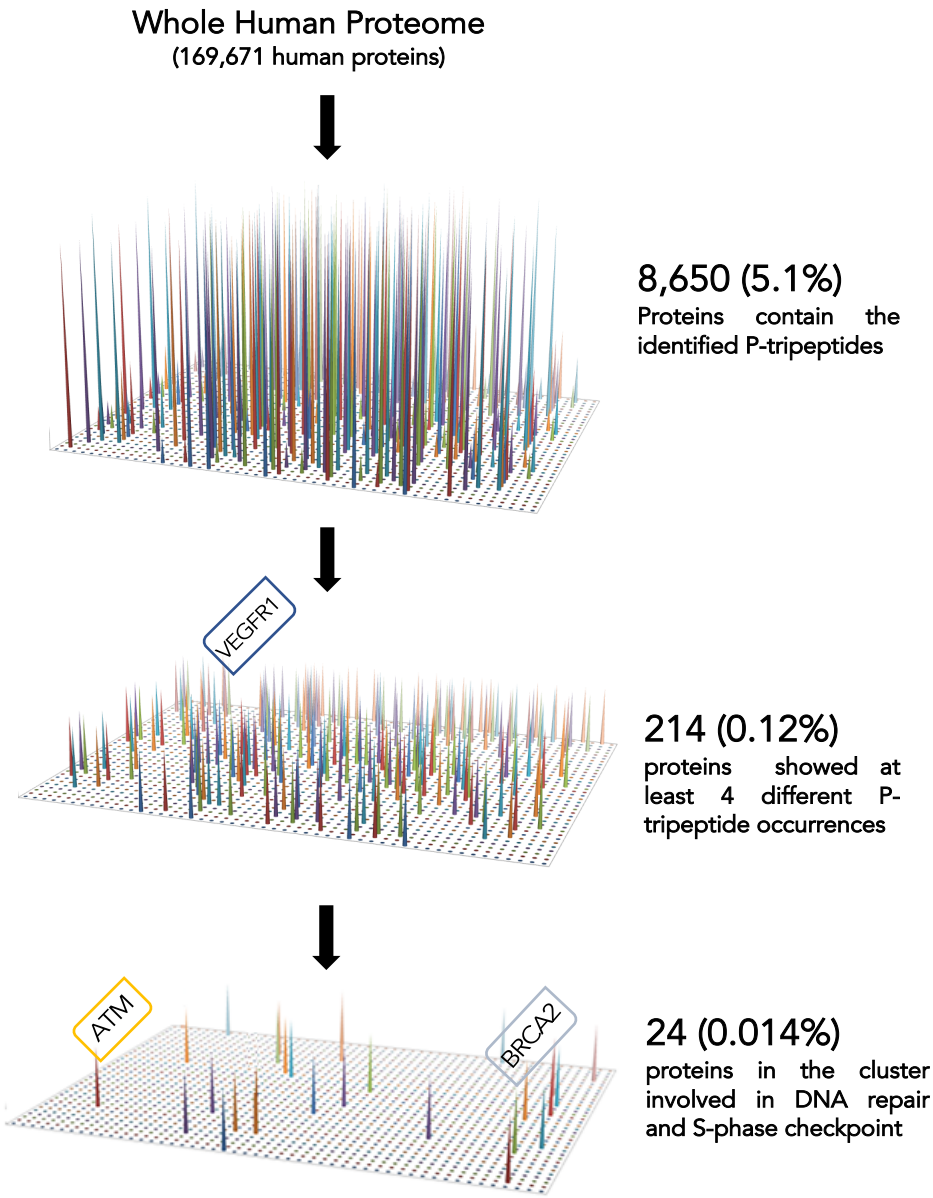


**Figure S2. Procedural scheme of P-tripeptide screening in the human proteome, (Related to Figure 1).** The exact distribution of each P-tripeptide in all human proteins annotated in the UniProt/SwissProt database (analysis performed in December 2018; https://www.uniprot.org) was analyzed using the Peptide search tool (https://www.uniprot.org/peptidesearch/). The entire human proteome was scanned to search for exact matches of each P-tripeptide. Among 8,650 proteins containing the identified tripeptides, only 214 showed at least 4 different tripeptide occurrences. These 214 proteins represented our starting subset to analyze potential candidates as new SMYD3 interactors. Next, we clustered these 214 proteins based on their biological function annotated in the corresponding Uniprot entry and confirmed the clustering in the Reactome database (e.g. HR pathway, Reactome id: R-HSA- 5685942; http://reactome.org). In the subset of 214 proteins showing at least 4 different tripeptide occurrences, we observed an enrichment in factors (24 proteins) involved in DNA repair and S- phase checkpoint (e.g. ATM, BRCA2).

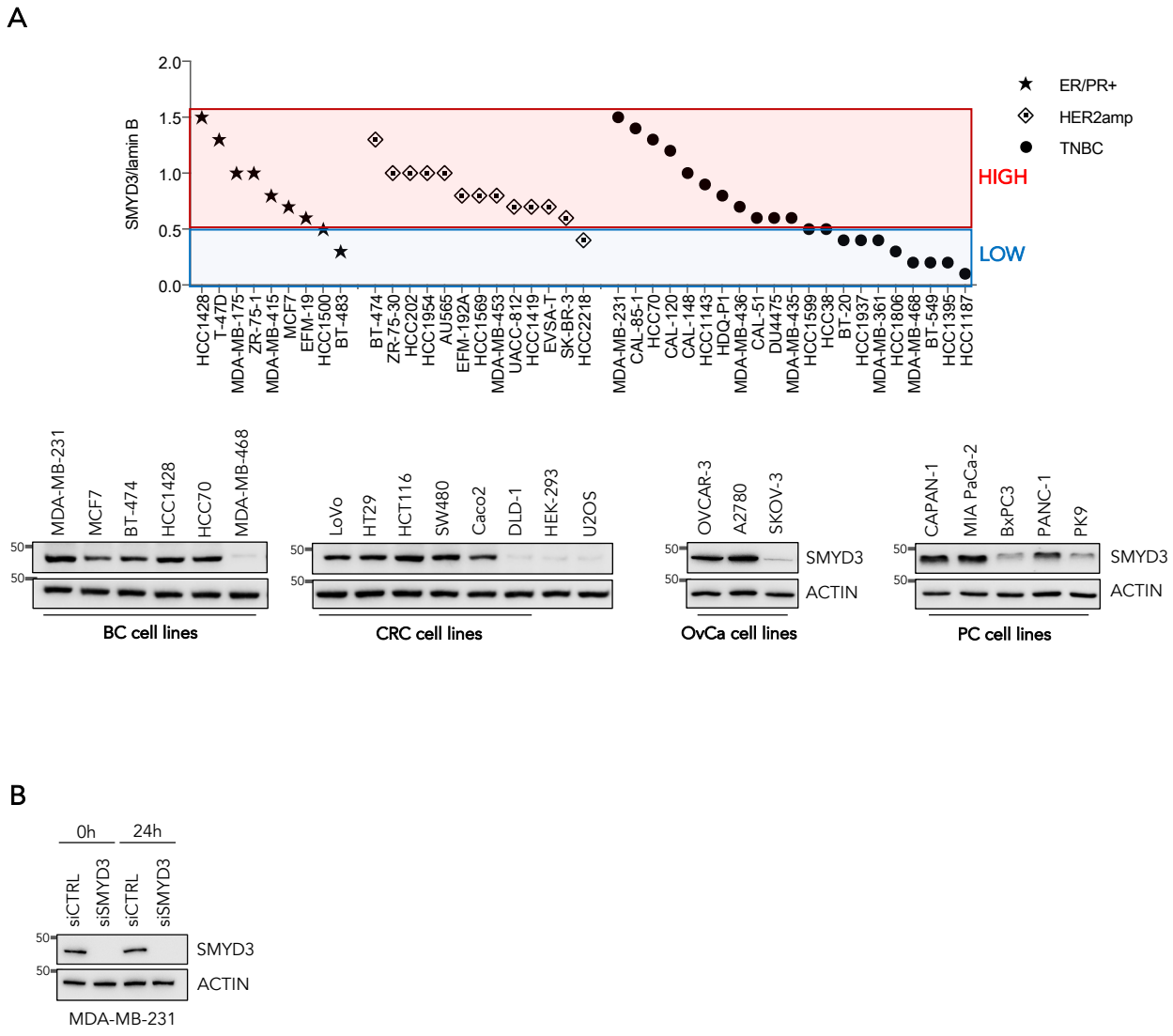


**Figure S3. Analysis of SMYD3 protein levels in BC cell lines (Related to Figures 2, 4, 5, 6, 7).**
(A) Upper panel: Densitometric analysis of SMYD3 levels, normalized against the loading control, in 43 BC cell lines classified for estrogen (ER) or progesterone (PR) receptor positivity and human epidermal growth factor receptor 2 (HER2) status; TNBC: triple-negative breast cancer cell lines without any marker positivity. Lower panel: immunoblotting analysis of SMYD3 protein levels in all the cell lines used in this study.
(B) Immunoblotting analysis of SMYD3 protein levels in MDA-MB-231 cells transfected with siCTRL and siSMYD3 depicted in Figure 2A. Actin was used as a loading control.

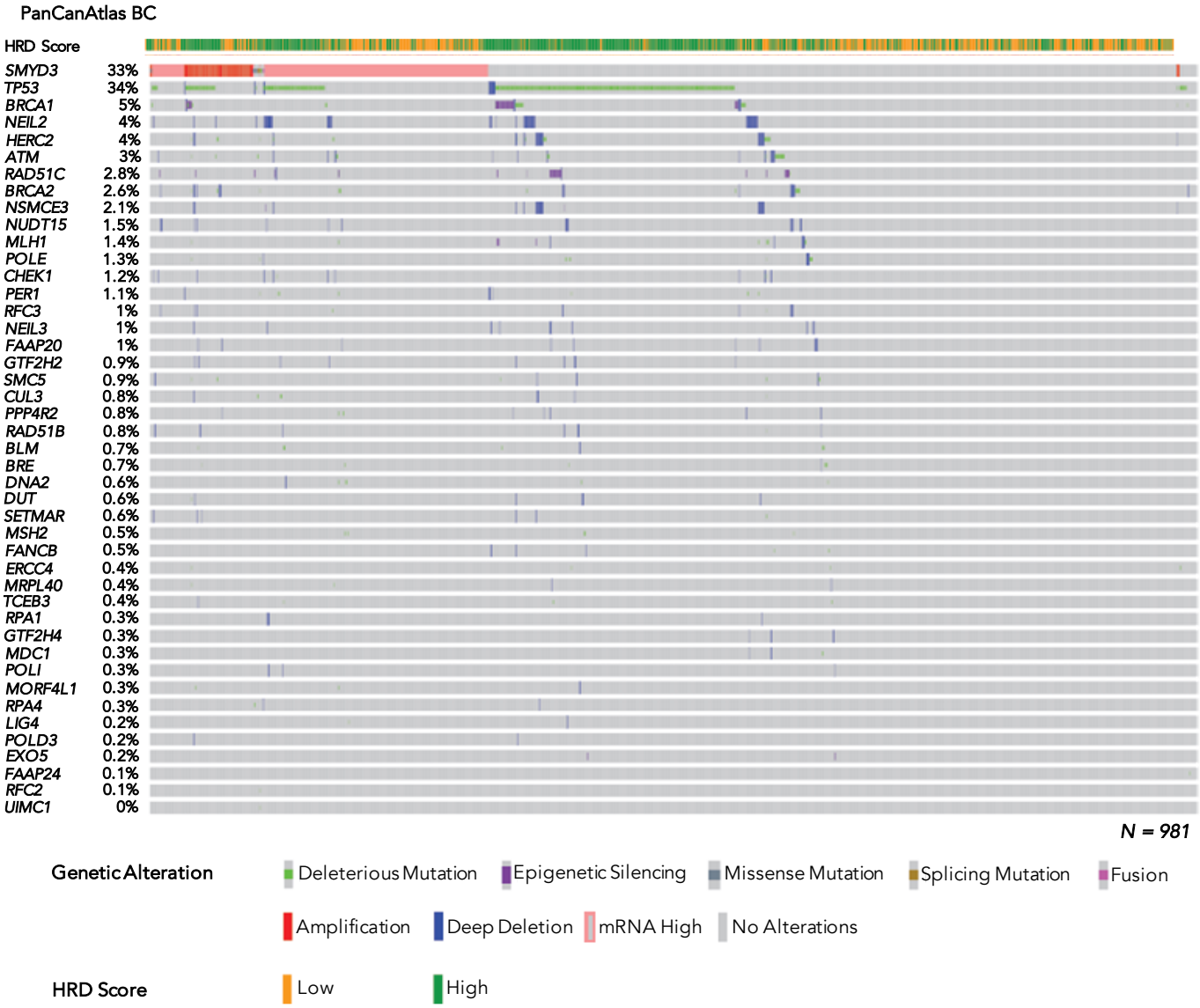


**Figure S4. Oncoprint of SMYD3 and HRD-associated genes in PanCanAtlas BC tumors, (Related to Figures 3, 8).**

Overall profiling of 981 BC tumors (columns) carrying alterations involving the SMYD3 gene (mRNA overexpression (25%), copy number alterations (6.7%), and mutations (1.12%) and deleterious mutations, deletions, and epigenetic silencing events for each HRD-associated gene (rows with gene names listed on the left). The association between BC tumors and the HRD score, low (≤ 21) and high (> 21), is represented as yellow and green bars, respectively. Grey boxes indicate the absence of alterations, and color/shape combinations corresponding to the various alteration types are indicated below the oncoprint. The frequency of each gene alteration in the oncoprint plot is indicated on the left.

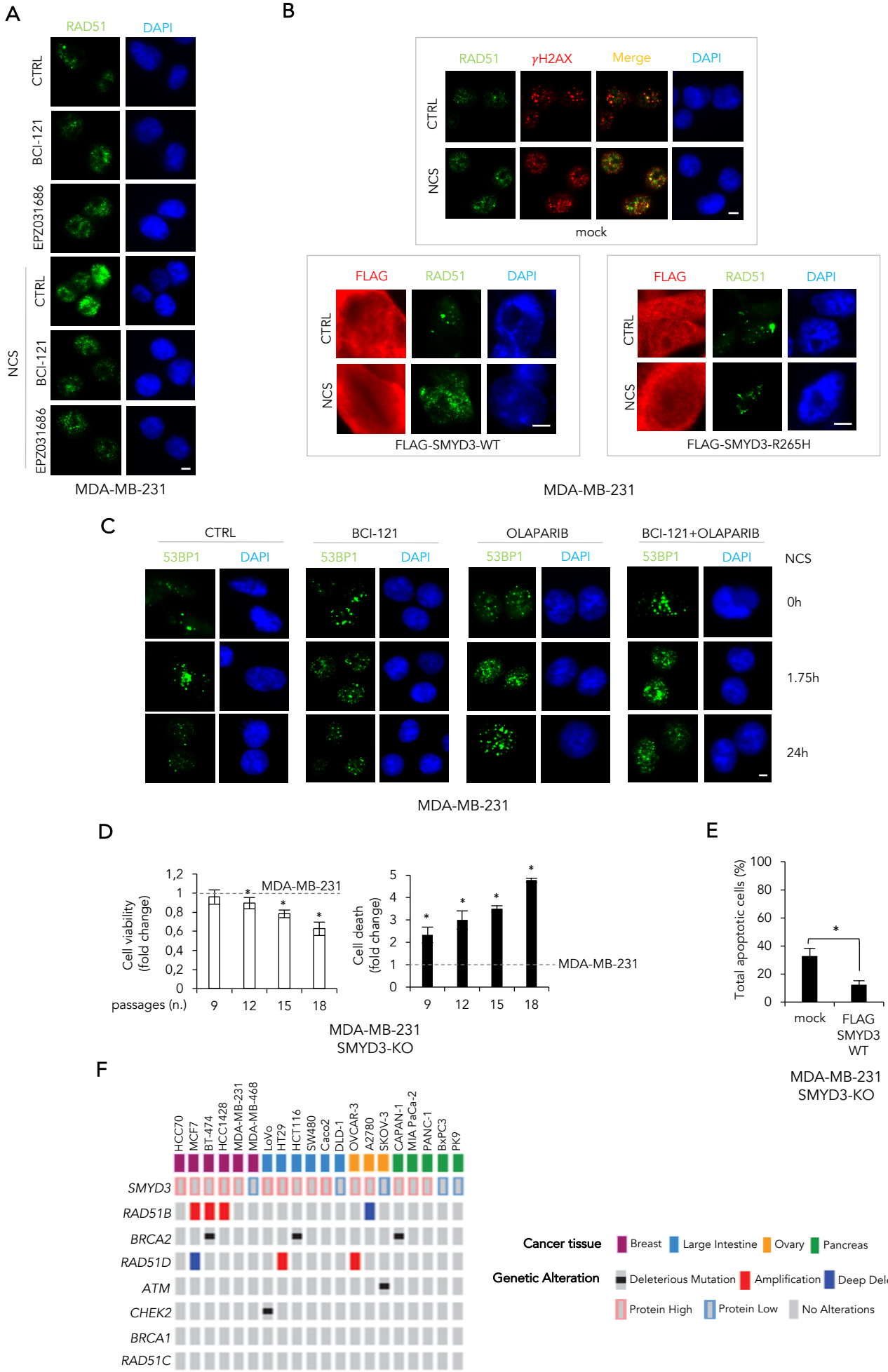
A
RAD51
DAPI
CTRL
BCI-121
EPZ031686
NCS
CTRL
BCI-121
EPZ031686
MDA-MB-231
B
RAD51
γH2AX
Merge
DAPI
CTRL
NCS
mock
FLAG
RAD51
DAPI
CTRL
NCS
FLAG-SMYD3-WT
FLAG-SMYD3-R265H
MDA-MB-231
C
CTRL
BCI-121
OLAPARIB
BCI-121+OLAPARIB
53BP1
DAPI
NCS
0h
1.75h
24h
MDA-MB-231
D
Cell viability (fold change)
MDA-MB-231
passages (n.)
9
12
15
18
Cell death (fold change)
MDA-MB-231
MDA-MB-231
SMYD3-KO
E
Total apoptotic cells (%)
mock
FLAG SMYD3 WT
MDA-MB-231
SMYD3-KO
F
HCC70
MCF7
BT-474
HCC1428
MDA-MB-231
MDA-MB-468
LoVo
HT29
HCT116
SW480
Caco2
DLD-1
OVCAR-3
A2780
SKOV-3
CAPAN-1
MIA PaCa-2
PANC-1
BxPC3
PK9
SMYD3
RAD51B
BRCA2
RAD51D
ATM
CHEK2
BRCA1
RAD51C
Cancer tissue
Breast
Large Intestine
Ovary
Pancreas
Genetic Alteration
Deleterious Mutation
Amplification
Deep Deletion
Protein High
Protein Low
No Alterations

**Figure S5. Characterization of SMYD3 role in DSB repair and mutation profiling in cancer cells, (Related to Figures 1, 5, 6, 7).**

(A) Immunostaining for RAD51 (green) in MDA-MB-231 cells pre-treated for 4 h with BCI-121 (30 μM) or EPZ031686 (1 μM) and then subjected to DNA damage with NCS (1 nM) for 6 h. Nuclei were stained with DAPI (blue).

(B) Immunostaining of MDA-MB-231 cells treated with NCS (1 μM) for 6 h. Left panel: Immunostaining for RAD51 (green) and γH2AX (red) in untransfected MDA-MB-231 cells. Right panel: Immunostaining for RAD51 (green) and FLAG (red) in MDA-MB-231 cells transfected with FLAG-SMYD3-WT or FLAG-SMYD3-R265H. Nuclei were stained with DAPI (blue).

(C) Immunostaining for 53BP1 (green) in MDA-MB-231 cells pre-treated for 4 h with BCI-121 (30 μM) and/or olaparib (10 μM) and then exposed to NCS (1 nM) for 24 h. Nuclei were stained with DAPI (blue). (A,B,C) The scale bar represents 5 μm.

(D) Quantification of cell viability and cell death by trypan blue staining in SMYD3-KO MDA-MB-231 cells at the indicated culture passages, normalized against wild-type MDA-MB-231 cells.

(E) Cell death analysis by annexin V staining. SMYD3-KO MDA-MB-231 cells were transfected with FLAG-SMYD3-WT for 24 h and then analyzed by flow cytometry for annexin V staining. The indicated percentages of total apoptotic cells include early and late apoptotic and dead cells.

(D, E) Statistical analysis was performed using Student's t-test; $*p \leq 0.05$. Results are representative of at least three independent experiments.

(F) Mutation profiles of selected BC, CRC, OvCa, and PC cell lines.

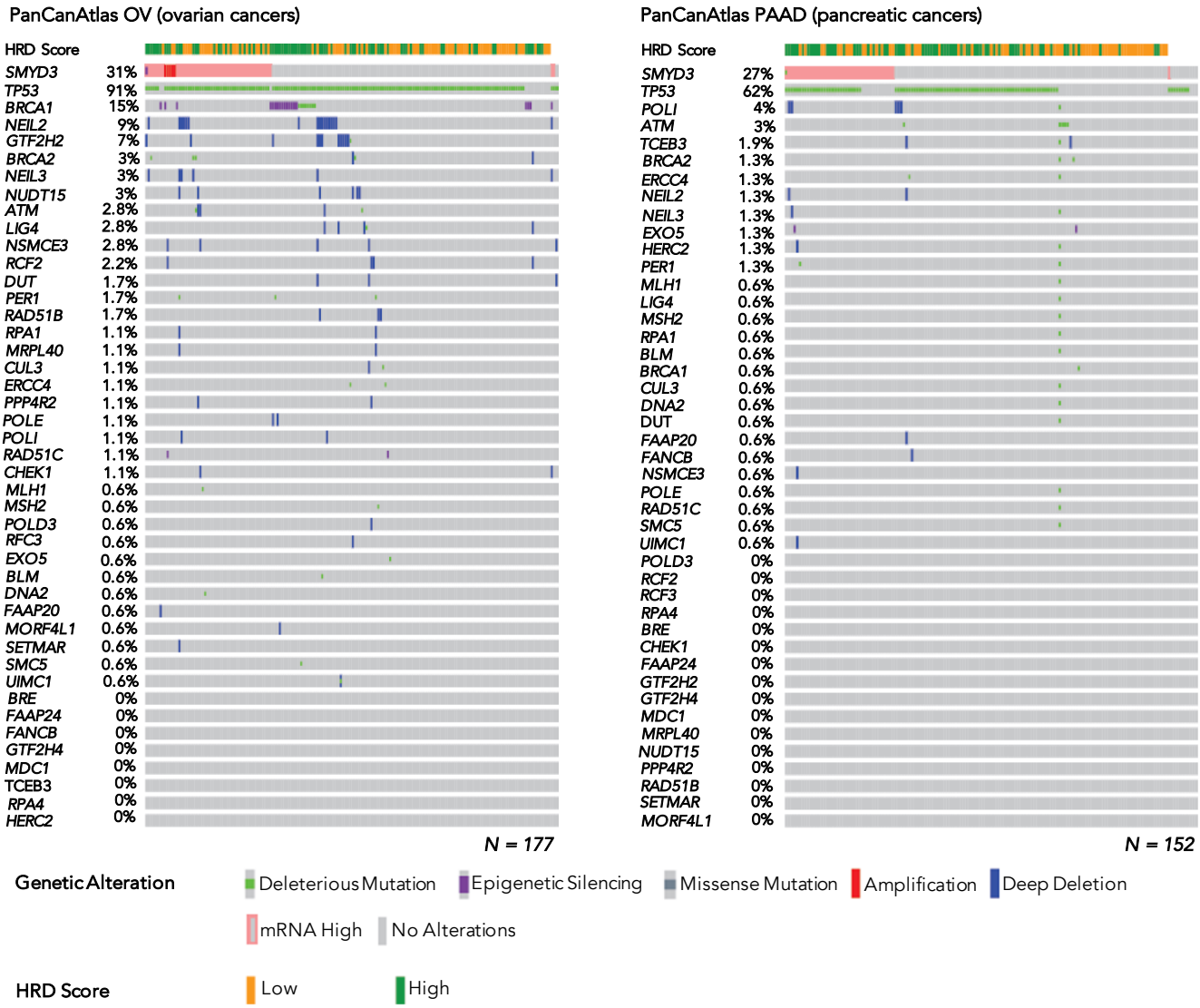


**Figure S6. Oncoprint of *SMYD3* and HRD-associated genes in PanCanAtlas OV and PAAD tumors, (related to Figure 8).**

Overall profiling of 177 OV and 152 PAAD tumors (columns) carrying alterations involving the *SMYD3* gene mRNA overexpression and deleterious mutations, deletions, and epigenetic silencing events for each HRD-associated gene (rows with gene names listed on the left). The association between tumors and the HRD score, [OV: low (≤ 44) and high (> 44); PAAD: low (≤17) and high (>17)], is represented as yellow and green bars, respectively. Grey boxes indicate the absence of alterations, and color/shape combinations corresponding to the various alteration types are indicated below the oncoprint. The frequency of each gene alteration in the oncoprint plot is indicated on the left.

| | SMYD3 STATUS | IHC intensity | % positive cells | Localization |
|---|---|---|---|---|
| Proband (BC 39y) | p.Arg265His | 3 | 95 | cytoplasmic and nuclear |
| Father (BC 54y) | p.Arg265His | 3 | 95 | cytoplasmic |
| Paternal aunt (BC 43y) | p.Arg265His | 3 | 95 | cytoplasmic and nuclear |
| Paternal aunt (BC 50y) | Wild-type | 3 | 70 | cytoplasmic |

**Table S1: SMYD3 immunohistochemistry results in the analyzed BC family, (Related Figure 3).**

| | Gene 1 | Gene 2 | P-value | Q-value |
|---|---|---|---|---|
| BC | TP53 | SMYD3 | 1.236261e-22 | 1.236261e-22 |
| | BRCA1 | SMYD3 | 3.264069e-09 | 6.215379e-09 |
| | NEIL2 | SMYD3 | 1.315987e-02 | 2.186762e-02 |
| | HERC2 | SMYD3 | 5.295595e-05 | 1.501736e-04 |
| | ATM | SMYD3 | 1.214102e-03 | 2.226760e-03 |
| | RAD51C | SMYD3 | 8.720251e-04 | 1.431774e-03 |
| | BRCA2 | SMYD3 | 5.848456e-04 | 1.016715e-03 |
| COAD-READ | MLH1 | SMYD3 | 2.5344277e-08 | 5.753839e-08 |
| | ATM | SMYD3 | 1.019042e-04 | 1.101908e-04 |
| | EXO5 | SMYD3 | 3.064239e-09 | 7.806982e-09 |
| | HERC2 | SMYD3 | 2.499592e-06 | 3.315551e-04 |

**Table S2: Results of mutual exclusivity analysis in PanCanAtlas BC and COAD-READ tumors, (Related Figure 8).**

P-values and Q-values were obtained using the DISCOVER's mutual exclusivity test.

## Transparent Methods

### Clinical data

A high-risk, BRCA1/2 mutation-negative breast cancer (BC) family (Figure 3B) from the Italian Multicenter Study on Male BC (MBC) was selected for whole-exome sequencing (Rizzolo et al., 2019). The proband, a man affected by BC, was diagnosed at the age of 39 years with an estrogen/progesterone receptor-positive ductal carcinoma *in situ* and at the age of 48 years with an estrogen/progesterone receptor-positive invasive ductal carcinoma. His father was diagnosed with invasive BC at the age of 54 years; both paternal aunts were diagnosed with BC at 43 and 50 years, respectively.

### Cell Lines

HEK-293, HCT116, MDA-MB-231, MDA-MB-468, MDA-MB-175, MDA-MB-415, MDA-MB-453, MDA-MB-436, MDA-MB-435, MDA-MB-361, HT29, MCF7, BT-474, BT-483, BT-20, DU4475, HCC1428, HCC1500, HCC1599, HCC38, HCC70, HCC202, HCC1954, HCC1143, HCC1187, HCC2218, HCC1806, HCC1419, HCC1937, HCC1569, DLD-1, LoVo, Caco2, OVCAR-3, A2780, SKOV-3, BxPC3, PK9, CAPAN-1, PANC-1, MIAPaCa-2, SW1990, SW480, T-47D, ZR-75-1, ZR-75-30, AU565, UACC-812, and SK-BR-3 cells lines were purchased from ATCC. CAL-85-1, CAL-148, CAL-51, CAL-120, EFM-19, EFM192A, Evsa-T, and HDQ-P1 cell lines were purchased from DSMZ. The U2OS cell line was kindly provided by Prof. Jeremy Stark. The SMYD3-KO MDA-MB-231 cell line was created using the CRISPR/Cas9 technology.
HEK-293, HCT116, MDA-MB-231, MDA-MB-468, HT29, MCF7, MDA-MB-231-SMYD3 KO, SW480, SW1990, OVCAR-3, SKOV-3, PANC-1, MIAPaCa-2, CAL-120, Evsa-T, SK-BR-3, HDQ-P1, and U2OS cells were cultured in DMEM high glucose (HG), without pyruvate (#11360-070, Gibco) with 10% FBS (#0270-106, Gibco) and 100 IU/ml penicillin-streptomycin (#15140-122, Gibco). HCC1428, MDA-MB-175, MDA-MB-415, MDA-MB-453, MDA-MB-436, MDA-MB-435, MDA-MB-361, UACC-812, CAL-85-1, CAL-148, CAL-51, BT-20, and BT-474 cells were maintained in the same conditions with 1% NEAA (#11140, Sigma Aldrich). LoVo cells were cultured in DMEM high glucose (HG) with 20% FBS and 100 IU/ml penicillin-streptomycin. Caco2 cells were maintained in the same conditions with 1% NEAA (#11140, Sigma Aldrich) and HEK-293 cells were supplemented with 1% pyruvate (#11360070, Gibco) and 1% NEAA (#11140, Sigma Aldrich). DLD-1, A2780, BxPC3, PK9, T-47D, ZR-75-1, ZR-75-30, EFM-19, EFM192A, HCC1428, HCC1500, HCC1599, HCC38, HCC70, HCC202, HCC1954, HCC1143, HCC1187, HCC2218, HCC1806, HCC1419, HCC1937, HCC1569, BT-483, AU565, DU4475, and CAPAN-1 cells were cultured in RPMI high glucose (HG), without pyruvate (#21875-034, Gibco) with 10% FBS (Gibco) and 100 IU/ml penicillin-streptomycin (Gibco). All cell lines were tested to be mycoplasma-free (#117048; Minerva Biolabs) at multiple times throughout the study. All cell culture was performed in a 37°C and 5% $CO_2$ incubator.

### E. coli

Tuner™(DE3) Competent Cells (#70623) were obtained from Novagen and were grown in standard LB media. High-Efficiency DH5α Competent Cells (C2987H) obtained from New England Biolabs were used for all cloning experiments performed in this study. Cells were grown in standard LB media.

### Chemicals

Neocarzinostatin (N9162), BCI-121 (SML1817), and Doxorubicin (D1515) were purchased from Sigma-Aldrich. KU60019 (S1570), and Olaparib (S1060) were purchased from SelleckChem. EPZ031686 (HY-19324) was purchased from MedChemExpress.
For each chemical, doses and treatment duration are indicated in the figure legends.

### Peptides

Peptides were purchased from Proteogenix. Peptides were delivered in lyophilized form and obtained at a

purity of at least 95% with TFA removal and in the hydrochloride salt form. The peptides used in this work are listed below.
P1-tripeptide: NFF, P2-tripeptide: DFF, P3-tripeptide: LFF, P4-tripeptide: FFF, P5-tripeptide: QFF, P6-tripeptide: KFF, P7-tripeptide: NIF, P8-tripeptide: NYF, P9-tripeptide: NAF, P10-tripeptide: NDF, P11-tripeptide: NHF, P12-tripeptide: NNF, P13-tripeptide: NFI, P14-tripeptide: NFY, P15-tripeptide: NFA, P16-tripeptide: NFH, P17-tripeptide: NFW, P18-tripeptide: NFR, P19-tripeptide: NFK.

**Plasmids**

The plasmids described in the manuscript were generated with specific primers, as previously described (Nakatani Y et al., 2003**)**. Site-directed mutagenesis was performed using the Q5® Site-Directed Mutagenesis Kit (#E05545, New England Biolabs) according to the manufacturer's instructions.
The p3xFLAG-CMV14-SMYD3-WT construct was generated starting from the SMYD3 cDNA ORF Clone in Cloning Vector, Human (HG11217-M, Sino Biological), used as a template to amplify SMYD3. HindIII-SMYD3 FW *5′-CTAAAGCTTATGGAGCCGCTGAAG* and EcoRI-SMYD3 RV *5′-ATTACGAATTCTGGGATGCTCTGATGT* primers were used for the PCR. The SMYD3 fragment was cloned into the p3xFLAG-CMV14 EMPTY plasmid (E7908, Sigma) linearized with HindIII and EcoRI.
The pCMV14-SMYD3-WT-HAHA construct was generated starting from the pHAHA EMPTY (#12517, Addgene) plasmid, used as a template to amplify HAHA. KnpI-HA FW *5′-TGGTTGGTACCTGGATACGATGTTCCAGATTACGCT* and XbaI-stop-HA RV *5′-GGATCCTCTAGATGTATCTTATCATGTCTGGATCCGGC* primers were used for the PCR. The HAHA-stop codon fragment was cloned into the p3xFLAG-CMV14-SMYD3-WT plasmid linearized with KnpI and XbaI.
The pCMV14-SMYD3-R265H-FLAG construct was generated by site-directed mutagenesis, using SDM SMYD3 R265H FW *5′-P-GTGACTGTTTCCATTGCCAAACCCAGG* and SDM SMYD3 R265H RV *5′-P-ATTCAAAGCAGTACTGGTCCCTCAGC* primers.
The p3xFLAG-CMV14-SMYD3-WT-HAHA-SMYD3-R265H-FLAG construct was generated starting from p3xFLAG-CMV14-SMYD3-R265H, used as a template to amplify CMV14-SMYD3-R265H-FLAG. XhoI CMV FW *5′-AATCGCTCGAGTGATGCGGTTTTGGCAGTA* and XbaI-SMYD3 RV *5′-TACTCTAGAGGATGCTCTGATGTTGGC* primers were used for the PCR. The CMV14-SMYD3-R265H-FLAG fragment was cloned into the pCMV14-SMYD3-WT-HAHA plasmid linearized with XhoI and XbaI.
pCS2-MYC-SMYD3-WT was generated as previously described in Proserpio et al., 2013.
pCDNA-FLAG-CHK2 was generated as previously described in Zannini et al., 2003.
GST-BRCA2 fragments (B2-1 to B2-9) cloned into the pGEX-4T3-GST vector were kindly provided by Professor Ashok Venkitaraman (MRC Cancer Unit, Cambridge, UK). GST-ATM fragments (A1 to A8) cloned into the pGEX-4T2-GST vector were kindly provided by Professor Titia de Lange (The Rockefeller University, New York, USA). GST-HSP90 C (616-736) (#22483), pCDNA3.1(+)-HIS-FLAG-ATM (#31985) and pET28-MHL-SMYD3-WT (#32048) were purchased from Addgene**.**

**Cell transfection and RNA interference**

U2OS cells were co-transfected with pCBASceI (#26477, Addgene) and p3xFLAG-CMV14-SMYD3-WT or p3xFLAG-CMV14-SMYD3-R265H using Lipofectamine 3000 (#L3000015, Thermo Fisher Scientific) according to the manufacturer's instructions.
MDA-MB-231 cells were transiently transfected with mammalian expression plasmids using fectamine 3000 (L3000015, Thermo Fisher Scientific) according to the manufacturer's instruction. For RNA interference, MDA-MB-231 cells were transfected with 50 nM validated siRNAs (Eurofins) directed against SMYD3 by using the HiPerfect reagent (#301704, QIAGEN) according to the manufacturer's instructions. siCTRL (Eurofins) was used as a non-silencing control. siRNA sequences used in this study:
siSMYD3: 5'-GAU UGA AGA UUU GAU UCU A
siCTRL: 5'-GCG UUG CUC GGA UCA GAA A

**CRISPR/Cas9 system**

The CRISPR/Cas9 reporter vector, GeneArt CRISPR Nuclease Vector Kit (#A21175, Invitrogen), was used according to the manufacturer's instructions. The *SMYD3* gene was analyzed with the CRISPR Search and

Design Tool (Thermo Fisher Scientific), which identified three different gRNA: gRNA1 top strand *5′-TTGCACACCGTGTACGCCAgtttt*, gRNA1 bottom strand *5′-TGGCGTACACGGTGTGCAAGcggtg,* gRNA2 top strand *5′-TTGGCGTACACGGTGTGCAgtttt,* gRNA2 bottom strand *5′-GCACACCGTGTACGCCAAGcggtg,* gRNA3 top strand *5′-AGTTCGCAACCGCCAAGAGgtttt,* gRNA3 bottom strand *5′-CTCTTGGCGGTTGCGAACTTcggtg.*
MDA-MB-231 cells were transfected with all-in-one expression vector Cas9-CD4$^{+}$-SMYD3 gRNA using Lipofectamine 3000 (L3000015, Thermo Fisher Scientific) according to the manufacturer's instruction. After 48 h MDA-MB-231 CD4$^{+}$ cells were enriched using the Dynabeads CD4 Positive Isolation Kit (11331D, Thermo Fisher) according to the manufacturer's instructions. Isolation of clonal populations was performed with agarose-based cloning rings (#C1059, Sigma). Cell clones were tested for site-specific loss of function alterations by PCR, using SMYD3 gRNA sequencing FW *5′-AGCCCGTGAGACGCCCGCTGCTGG* and SMYD3 gRNA sequencing RV *5′-GAAAAGTTCGCAACCGCCAA*. Sequencing products were purified using the Dye Ex 2.0 Spin Kit (#63204, QIAGEN) and sequenced on an ABI PRISM 310 Genetic Analyzer (Applied Biosystems).

**Recombinant protein expression/purification**

Tuner™(DE3) Competent Cells, transformed with different constructs, were grown in Luria Broth medium with Ampicillin (A9518, Sigma), Chloramphenicol (C0378, Sigma), and 0,5 mg/ml L-(+)-Arabinose (A3256, Sigma) and induced with 1 mM IPTG when they reached the optical density of 0.6 (A600) at 37°C, for 3 h. Cells were then collected by centrifugation, and pellets were lysed with B-PER lysis buffer (#78248, Thermo Fisher Scientific). The lysate was centrifuged at 20,000 × *g* for 20 min at 4°C. Recombinant protein expression was confirmed by SDS-PAGE. GST-Fusion proteins were purified by Pierce Glutathione Magnetic Agarose Beads (78601, Thermo Fisher Scientific) according to the manufacturer's instructions. GST-fused proteins were evaluated and quantified by SDS-PAGE. HIS-Fusion proteins were purified by Dynabeads HIS-Tag Isolation and Pulldown (10104D, Thermo Fisher Scientific) according to the manufacturer's instructions. HIS-fused proteins were evaluated and quantified by SDS-PAGE.

**Immunoblotting**

Whole-cell extracts were obtained from cells collected and homogenized in lysis buffer (50 mM Tris-HCl pH 7.4, 5 mM EDTA, 250 mM NaCl, and 1% Triton X-100) supplemented with protease and phosphatase inhibitors (Roche). Nuclear fractions were obtained by using the Nuclear Extraction Kit (#ab113474, Abcam) according to the manufacturer's instructions. 20 µg of protein extracts from each sample were denatured in Laemmli sample buffer and loaded into an SDS-poly-acrylamide gel for immunoblot analysis. Primary antibodies used: 53BP1 (#4937, Cell Signaling), ATM (#2873, Cell Signaling), ACTIN ( #3700, Cell Signaling), BRCA2 (OP95, Merck), CHK2 (#6334, Cell Signaling), FLAG M2 (F1804, SIGMA), GAPDH (#2118, Cell Signaling), GST (#2625, Cell Signaling), HA-tag (H3663, SIGMA), MYC-tag (#2278, Cell Signaling), p-Ser/Thr ATM/ATR (#2851), PARP p85 Fragment (G7341, Promega), pATM (Ser1891) (#5883 Cell Signaling), polyHistidine (H1029, Sigma), RAD51 (#8875, Cell Signaling), SMYD3 (D2Q4V) (#12859, Cell Signaling), yH2AX (#9718, Cell Signaling) and LAMIN B1 (#12586S, Cell Signaling). Rabbit IgG HRP and Mouse IgG HRP (#NA934V, #NA931V, GE Healthcare) were used as secondary antibodies and revealed using the ECL-plus chemiluminescence reagent (GE Healthcare). Densitometric evaluation was performed by ImageJ software (Schneider et al., 2012).

**Co-immunoprecipitation (Co-IP)**

Cells were lysed with the Nuclear Extraction Kit (ab13474, Abcam), according to the manufacturer's instructions. 10% of the nuclear fractions was used as input. 1 µg of each antibody was coupled to Dynabeads Protein A (10002D, Thermo Fisher Scientific) or G (10004D, Thermo Fisher Scientific) in 100 µl of 0.01% Tween20-1X PBS for 45 min at room temperature on a rocking platform. Nuclear fractions were incubated with antibody-Dynabeads Protein A or G complexes for 1 h at room temperature on a rocking platform. Immunocomplexes were washed extensively, boiled in Laemmli sample buffer, and subjected to SDS-PAGE and immunoblot analysis. Primary antibodies used: MYC-tag (#2278, Cell Signaling), BRCA2 (OP95, Merk Millipore), FLAG (F1804, Sigma) and ATM (#2873, Cell Signaling). IgG was used as a negative control.

For endogenous co-immunoprecipitation, cells were lysed with the Nuclear Extraction Kit (ab13474, Abcam), nuclear fractions were digested or not in 1x Micrococcal Nuclease Reaction buffer with 0,1 U/µL of MNase (M0247S, New England Biolabs) for 5 min at 37°C. 1 µg of SMYD3 antibody (#12859, Cell Signaling Technologies) was coupled to Dynabeads Protein A (10002D, Thermo Fisher Scientific) and co-immunoprecipitation was carried on as described above.

**DR-GFP reporter assay**

U2OS-DR-GFP cells were seeded in 6 cm cell culture plates ($1x10^6$ cells/plate) and after 24h they were transfected with SceI-BFP, SceI-BFP+SMYD3_WT and SceI-BFP+SMYD3_R265H expressing vectors, using Lipofectamine 3000 transfection reagent (L3000015, Thermo Scientific, USA) according to manufacturer's instructions. After 24 h, cells were detached from plates by using 0.25% Tyripsin-EDTA (TD-4049-100, Sigma,USA), centrifuged at 1000 rpm x 10 min and suspended in an appropriate volume of cold flow cytometry buffer (phosphate buffer saline supplemented with 1% BSA). Cells were analyzed by using FACS Aria II fluorescence activated cell sorter (Beckton Dickinson, USA).

**Annexin V staining**

Briefly, $1\times10^6$ cells were cultured in 6-well plates (Corning Costar, Corning) for 72 h at 37°C, 5% CO2, with complete medium. After 24 h, cells were pre-treated or not for 48 h with BCI-121 or EPZ031686 and then treated or not with olaparib and/or with BCI-121 or EPZ031686 for another 24 h. $2\times10^4$ cells/plate were collected and resuspended in 1X PBS-1% FBS, then the Muse Annexin V and Dead Cell reagent was added to each tube (MCH100105, Luminex). Cells were incubated at room temperature for 20 min in the dark. Flow cytometry was performed using the Guava Muse Cell Analyzer. Cells were considered apoptotic if they were Annexin V+/PI- (early apoptotic) and Annexin V+/PI+ (late apoptotic). Each analysis was performed evaluating at least 2000 events using the assay-specific software module included in the Guava Muse Cell Analyzer instrument.

**Colony formation assay**

Colony formation assays were performed as previously described (Germani et al., 2014). Briefly, cells were cultured in 24-wells in the presence or absence of the indicated drugs. After 72 h, media were discarded and cells were washed twice with 1X PBS. An aliquot of 2 ml of Coomassie brilliant blue (#161-0400, BIORAD) was added into each dish for 5 min and then cells were washed with 1X PBS to remove excess Coomassie. Plates were dried at room temperature. Percent cell growth inhibition at each concentration was quantified by densitometric evaluation using ImageJ software (Schneider et al., 2012).

**Immunofluorescence and foci counting**

53BP1 (NB100-304, Novus Biologicals), γH2AX (05-636 Merck Millipore), FLAG (F1804, Sigma Aldrich), and RAD51 (#8875, Cell Signaling) foci were stained by immunofluorescence. Cells were grown on glass coverslips, treated as indicated for each experiment, and then fixed with 3% paraformaldehyde and 2% sucrose in 1X PBS for 10 min and permeabilized with 20 mM HEPES pH 7.6, 50 mM NaCl, 3 mM MgCl2, 300 mM sucrose, 0.2% Triton-X-100 for 5 min at room temperature. Glass coverslips were then blocked in 1X PBS, 3% BSA for 30 min, stained with primary antibody for 2 h at room temperature, then with Alexa Fluor secondary antibodies for 1 h at room temperature. Coverslips were mounted with medium anti-fading-containing DAPI to stain nuclei. Foci were scored by fluorescence microscopy using a 100X magnification objective and digital image acquisition on a Nikon Eclipse E1000 equipped with a DS-U3 CCD camera. The percentage of 53BP1 foci was calculated as follows: % residual damage = [(foci $t_{24h}$-foci $t_0$)/ (foci $t_{1.75h}$-foci $t_0$)] x 100.

**Cell viability and cell death**

Cell viability and cell death were assessed by counting. Briefly, supernatants (containing dead/floating cells) were collected. Cell pellets were resuspended in 1X PBS and 10 µl were mixed with an equal volume of 0.01% Trypan blue solution (T8154, Sigma-Aldrich). Viable cells (unstained, trypan blue-negative cells) and

dead cells (stained, trypan blue-positive cells) were counted with a phase-contrast microscope, and the percentages of viable and dead cells were calculated.

**DNA/RNA extraction, sequencing, and analysis**

DNA was extracted from both whole blood samples and microdissected FFPE sections of breast cancer tissue with commercial kits as previously reported (Silvestri et al., 2017).
Whole-exome sequencing of germline DNA samples from breast cancer tissue and subsequent data analysis were performed as previously described (Silvestri et al., 2017). Candidate variants were validated in germline and tumor DNA samples by double-stranded Sanger sequencing.
RNA was extracted from microdissected FFPE tumor sections using the MiReasy FFPE kit (217504, Qiagen) according to the manufacturer's instructions. RNA quality and quantity were assessed on a 2100 Bioanalyzer instrument (Agilent) (Wang et al., 2012). Libraries were prepared using the TruSeq RNA Access Library Prep kit (RS-301-2001, Illumina) according to the manufacturer's instructions. RNA-sequencing (75x2 bp) was performed on an Illumina NextSeq platform. A tailored bioinformatic pipeline including tools such as FastQC for quality control, STAR (version 2.5.1a) for alignment, and RSeQC-FPKM for counting reads was applied. Absolute quantification of transcripts (genes with all isoforms) was expressed in Fragments Per Kilobase of transcript per Million mapped reads (FPKM). The GATK Best Practices workflow for SNP and indel calling on RNA-seq data was used to evaluate the expression of variant alleles (Tian et al., 2016).

**Immunohistochemistry**

Tissue specimens were formalin-fixed in 4% buffered formalin and paraffin-embedded. Sequential sections (3 μm) were cut and used for morphological studies [stained with hematoxylin and eosin (HE)] and immunohistochemical analysis.
Sections were dewaxed and rehydrated in $dH_2O$. Endogenous peroxidase activity was blocked by incubation in 3% hydrogen peroxide for 10 min. Antigen retrieval was conducted in 10 mM sodium citrate buffer (pH 6.0) for 15 min. Sections were incubated overnight with the primary antibody, anti-SMYD3 (ab183498, Abcam, 1:200 dilution). Then, they were incubated with secondary biotinylated antibody and subsequently with streptavidin-biotin-peroxidase (UltraTek HRP Anti-Rabbit, Scy Tek). Samples were developed with DAB (ACH500, Scy Tek), counterstained with hematoxylin, and mounted with permanent mounting media. Negative controls were used in each experiment. SMYD3 immunoreactivity was evaluated by a semiquantitative approach by two independent pathologists, in a blinded manner, who scored the percentage of SMYD3-stained cells and the intensity of the staining (0: absent, 1: mild and focal, 2: moderate, 3: intense and diffuse).

**Chromatin immunoprecipitation (ChIP)**

Chromatin isolated from U2OS cells co-transfected with pCBASceI and p3xFLAG-CMV14-SMYD3-WT or p3xFLAG-CMV14-SMYD3-R265H was subjected to ChIP. Briefly, cells were cross-linked in 1% formaldehyde (F8775, Sigma Aldrich) for 10 min. After blocking cross-links with 0.125 M glycine for 5 min and washing with PBS, the pellet was resuspended in Farnham buffer (5 mM PIPES pH 8.0; 85 mM KCl; 0.5% NP-40). Cells were lysed in RIPA buffer (1× PBS; 1% NP-40; 0.5% sodium deoxycholate; 0.1% SDS). Chromatin was sonicated to a fragment length of about 1 kb and immunoprecipitated with 5 μg of rabbit IgG, anti-SMYD3 (NBP1-79393, NovusBio) or anti-RAD51 (14B4, cat. NB100-148, NovusBio) antibodies.
ChIP primers used:
DR-GFP+1300 FW: 5'- CCCCCGTAGCTCCAATCCTT
DR-GFP+1300 RV: 5'-CCAGGAGCGGATCGAAATTG
hChIP UbiquitB FW: 5'-GAAGGAAGAGAAGCGCATAGAGGAGAA
hChIP UbiquitB RV: 5'-CTCATAGCCGTAAGAAAGGCTCCTAAA
Quantitative real-time PCR was performed using SYBR green IQ reagent (Bio-Rad Laboratories) with the CFX Connect detection system (Bio-Rad Laboratories).

**Surface plasmon resonance (SPR)**

Direct binding assays were conducted employing flow-based SPR biosensor X100, (BIAcore, GE Healthcare) and data analysis was performed employing Scrubber or BIAevaluation software version 4.1. Recombinant human full-length SMYD3 was produced and purified in-house following a previously developed protocol (Peserico et al., 2015). Immobilization of SMYD3 on CM5 sensor chips was performed following a previously described amine-coupling procedure (Fabini et al., 2019). Briefly, using Hepes buffer saline (HBS) as running buffer, a 1:1 mixture of 0.4 M N-(3-Dimethylaminopropyl)-N'-ethylcarbodiimide (EDC) and 0.1 M N-hydroxy succinimide (NHS) was injected for 7 min over the sensor surface followed by 10 min injection of the recombinant human full-length SMYD3 diluted to 100 µg/ml. Remaining active esters were quenched by switching the running buffer to tris buffer saline containing 0.05% Tween-20 (TBS-T) supplemented with 2 mM dithiothreitol (DTT) and 2% DMSO. During the immobilization procedure, the flow rate was set at 10 µl/min. After the immobilization process, the surface was left to stabilize overnight to remove all tightly bound S-adenosyl methionine (SAM) which co-purifies with the protein. The whole process resulted in c.a. 8000 RU (Response Units) of SMYD3 covalently attached to the surface. For all performed experiments, the analysis temperature was set to 15°C. Interaction of tripeptides with immobilized SMYD3 was investigated using a 90 µl/min flow rate. Association was monitored for 30s and dissociation for 120s. All responses returned to baseline quickly after injection stopped, thus no regeneration procedure was necessary. A double-reference approach was used as negative control: the SPR signal was recorded upon injection of each tripeptide over the sensing surface bearing the immobilized SMYD3 and was corrected by the signal recorded in the reference cell and that of a blank solution. Reference cell allows accounting for non-specific interactions while signals recorded upon injections in both cells of a blank solution accounted for optical interference. RU values measured at the end of the injection phase were normalized for the molecular weight (MW) of each tripeptide to achieve MW-adjusted RUs. Interactions of tripeptides with immobilized SMYD3 were monitored both in SAM-free and SAM-supplemented buffer. SAH (S-adenosyl-homocysteine) was used as a positive control compound in the first instance while a 26-amino acid peptide, based on MAP3K2 sequence 249-274, was used in the latter. The total number of replicates was 2.

***In vitro* pull-down assay**

HIS-SMYD3-WT recombinant human protein was incubated with nine GST fusion proteins, designated B2-1 to B2-9, that span the entire coding region of BRCA2, or with eight GST fusion proteins, designated A-1 to A-8, that span the entire coding region of ATM, or with recombinant human CHK2 protein (ab42604, Abcam). HSP90 C (616-736) GST fusion protein was used as a positive control. HIS-SMYD3-WT recombinant protein (500 ng) and GST fusion proteins (200 ng) were incubated for 1 h at 4°C on a rocking platform for *in vitro* binding. These fusion proteins were precipitated by Dynabeads HIS-Tag Isolation and Pulldown (Thermo Fisher Scientific) according to the manufacturer's instructions, then washed extensively in buffer A (20 mM Tris-HCl pH 8, 150 mM KCl, 5 mM MgCl2, 0.2 mM EDTA, 10% glycerol, 0.1% NP-40) containing fresh inhibitors and 1 mM DTT. Afterward, the precipitates were resolved on 10% SDS-PAGE and subjected to immunoblot analysis. Primary antibodies used: polyHistidine (H1029, Sigma) and GST (#2625, Cell Signaling). Rabbit IgG HRP and Mouse IgG HRP (#NA934V, #NA931V, GE Healthcare) were used as secondary antibodies and revealed using the ECL-plus chemiluminescence reagent (GE Healthcare).
For the competition assay, 500 ng of HIS-SMYD3-WT recombinant protein and 200 ng of GST-BRCA2 B2-4 or GST-ATM A-8 fusion proteins were incubated for 1 h at 4°C on a rocking platform in the presence of escalating doses (0, 1, 5, 25, 125, 625 mM) of the purified P1 and P10 tripeptides, respectively. Bound proteins were precipitated and resolved as described above.

**ADP luminescent assay**

Analysis of ATM kinase activity was performed using a luminometric kinase assay by varying the concentration of ATP using the ADP-Glo reagents (#V6930, Promega). This luminescent ADP detection assay measures kinase activity by quantifying the amount of ADP produced during a kinase reaction. Briefly, ATM active protein (100 ng, #14-933 Millipore) was assayed in a kinase reaction buffer containing 40 mM Tris (pH 7.5), 20 mM MgCl2, 0.1 mg/ml BSA, varying concentrations of ATP, and 500 ng of human recombinant SMYD3-WT or SMYD3-R265H. After 30 min of incubation, an equal volume of ADP-Glo reagent was added to stop the kinase reaction and deplete the remaining ATP. Then, kinase detection reagent was added to convert ADP to ATP, which was determined by a luciferase/luciferin reaction. The generated

luminescence was measured using a luminometer. Each data point was collected in triplicate and the result is shown as fold change on active-ATM only.

**Prediction analysis**

P-tripeptide screening was performed *in silico* using the Uniprot Peptide search tool (https://www.uniprot.org/peptidesearch/) to identify potential candidates as new SMYD3 interactors. Each P-tripeptide was searched in all human proteins annotated in the Uniprot database (analysis performed in December 2018) and 8,650 proteins showed at least one identified tripeptide. Then, we analyzed the subset of all human proteins showing ≥ 4 P-tripeptide occurrences (214 proteins) for their biological function based on the functional annotation reported in the related Uniprot entry and in the Reactome database (i.e. HR pathway, Reactome id: R-HSA-5685942; https://reactome.org/; Fabregat et al., 2018; Jassal et al., 2020). Of note, we found that 24 proteins showing ≥4 P-tripeptide occurrences are involved in DNA repair and S-phase checkpoint pathways.

*In silico* prediction of SMYD3 phosphorylated sites was performed using three different tools: PhosphoELM (http://phospho.elm.eu.org/, Dinkel et al., 2011), DISPHOS (http://www.dabi.temple.edu/disphos/, Iakoucheva et al., 2004) and NetPhos (http://www.cbs.dtu.dk/services/NetPhos/, Bloom, et al., 2004). This analysis identified T268 as the best target site for phosphorylation by ATM.

**TCGA PanCanAtlas data source/meta-analysis**

The analysis of genomic alterations of PanCanAtlas breast invasive carcinoma (BC), colon and rectum adenocarcinoma (COAD, READ), pancreatic adenocarcinoma (PAAD) and ovarian serous cystadenocarcinoma(OV) tumors was performed using a published study carried out by integrating data on somatic truncating and missense mutations, copy number deletions defined by GISTIC, and epigenetic silencing events by The Cancer Genome Atlas (TCGA) DNA Damage Repair Analysis Working Group (Knijnenburg et al., 2018). The available binary calls for each event class for a curated list of 276 genes encompassing all major DNA repair pathways were used to assess the prevalence of 43 DNA damage repair (DDR) gene alterations (*LIG4*, *MLH1*, *MSH2*, *POLD3, RFC2*, *RFC3*, *RPA1*, *RPA4*, *ATM*, *BLM*, *BRCA1*, *BRCA2*, *BRE*, *CHEK1*, *CUL3*, *DNA2*, *DUT*, *ERCC4*, *FAAP24*, *FAAP20*, *FANCB*, *GTF2H2*, *GTF2H4*, *MDC1*, *MRPL40*, *NEIL2*, *NEIL3*, *NSMCE3*, *NUDT15*, *PER1*, *POLE*, *POLI*, *PPP4R2*, *RAD51B*, *RAD51C*, *SETMAR*, *SMC5*, *TCEB3*, *TP53*, *UIMC1*, *EXO5*, *MORF4L1*, and *HERC2*) with a significant positive homologous recombination deficiency (HRD) determined using Bayesian ridge regression to model HRD scoring as a function of DDR gene alterations. We retrieved from the same published article the HRD score, a measure obtained by combining three separate metrics of genomic scarring (HRD loss of heterozygosity, large scale transition, and the number of telomeric imbalances). We defined BC, COAD-READ, PAAD, and OV as low HRD scoring if the HRD score was below or equal the median within the relevant cancer type. The website cBioPortal (https://www.cbioportal.org; Gao et al., 2013; Cerami et al.,2012) was used for the meta-analysis. Somatic mutations, copy number alterations, and RSEM processed and Z-score RNA-Seq v2 gene expression data from PanCanAtlas BC (N=981), COAD-READ (N=459), PAAD (N=152), and OV (N=177) tumors that were comprehensively and systematically analyzed for 276 DDR genes were downloaded from cBioPortal (http://www.cbioportal.org) to characterize *SMYD3* somatic alterations. Patients were stratified based on *SMYD3* Z-score and the third quartiles were identified as high SMYD3 (BC, q3 SMYD3 Z-score ≥ 1.06, N=245), (COAD-READ, q3 SMYD3 Z-score ≥ 0.41, N=126), (PAAD, q3 SMYD3 Z-score ≥ 0.41, N=41), (OV, q3 SMYD3 Z-score ≥ 0.65, N=52).

**Mutual exclusion analysis**

Mutual exclusivity between *SMYD3* and HRD-associated genes was evaluated using the DISCOVER analysis tool (Sander et al., 2016). Overexpression of *SMYD3* mRNA and deleterious alterations of 43 HRD-associated genes from 981 BC, 459 COAD-READ, 152 PAAD, and 177 OV tumors were combined into a single *NxM* binary data matrix for each cancer type, where each cell value $V_{i,j}$ ($i = 1 \ldots N$ *[Number of genes]*, $j = 1 \ldots M$ *[Number of tumors]*) indicated the status of gene $i$ in tumor $j$. $V_{i,j} = 1$ if gene $i$ is mutated in tumor $j$ and 0 otherwise. The alteration status of all genes across all tumors for each cancer type was used to generate a null distribution for background alternation rate estimation. Finally, we computed pairwise mutual

exclusivity between any two genes mutated in more than two tumors, taking the null distribution into account.

**Cell line mutational analysis**

Somatic mutations and copy number alteration data of key HR-related genes (BRCA1, BRCA2, CHEK2, ATM, RAD51B, RAD51C, and RAD51D) were retrieved from the Cancer Cell Line Encyclopedia (CCLE, https://portals.broadinstitute.org/ccle; Ghandi et al., 2019) and the Catalogue of Somatic Mutation in Cancer (COSMIC, https://cancer.sanger.ac.uk/cosmic; Tate et al., 2019) databases to assess the mutational status of BC cell lines (CCLE: HCC70_BREAST, MCF7_BREAST, BT474_BREAST, HCC1428_BREAST, MDAMB231_BREAST, MDAMB468_BREAST), colon cancer cell lines (CCLE: LOVO_LARGE_INTESTINE, HT29_LARGE_INTESTINE, HCT116_LARGE_INTESTINE, SW480_LARGE_INTESTINE, CaCo2_LARGE_INTESTINE, DLD1_LARGE_INTESTINE), ovarian cancer cell lines (CCLE: NIHOVCAR3_OVARY, A2780_OVARY, SKOV3_OVARY,), and pancreatic cancer cell lines (CCLE: CAPAN1_PANCREAS, MIAPACA2_PANCREAS, PANC1_PANCREAS, BXPC3_PANCREAS; COSMIC: PK-9).

**QUANTIFICATION AND STATISTICAL ANALYSIS**

Data were analyzed and plotted using Microsoft Excel and GraphPad Prism softwares. Statistical analysis was performed using Student's t-test or one-way ANOVA followed by a Dunnett test. Differences were considered significant when $p \leq 0.05$. At least three independent experiments were performed for all of the assays.

## Supplemental References


Blom, N., Sicheritz-Pontén, T., Gupta, R., Gammeltoft, S., and Brunak, S. (2004). Prediction of post-translational glycosylation and phosphorylation of proteins from the amino acid sequence. Proteomics 4, 1633–1649.

Cerami E., Gao, J., Dogrusoz, U., Gross, B.E., Sumer, S.O., Aksoy, B.A, Jacobsen, A., Byrne, C.J., Heuer, M.L., Larsson, E., et al. (2012). The cBio cancer genomics portal: an open platform for exploring multidimensional cancer genomics data. Cancer Discov. 2, 401–404.

Dinkel, H., Chica, C., Via, A., Gould, C.M., Jensen, L.J., Gibson, T.J., and Diella, F. (2011). Phospho.ELM: a database of phosphorylation sites-update 2011. Nucleic Acids Research. 39, D261–D267.

Fabini E., Manoni E., Ferroni C., Del Rio, A., and Bartolini M. (2019). Small-molecule inhibitors of lysine methyltransferases SMYD2 and SMYD3: current trends. Future Med. Chem. 11, 901–921.

Fabregat A., Jupe S., Matthews L., Sidiropoulos K., Gillespie M., Garapati P., Haw, R., Jassal B., Korninger F., May B., Milacic, M., et al.(2018). The Reactome Pathway Knowledgebase. Nucleic Acids Res. 46, D649–D655.

Germani, A., Matrone, A., Grossi, V., Peserico, A., Sanese P., Liuzzi M., Palermo R., Murzilli S., Campese A.F., and Ingravallo G., et al. (2014). Targeted therapy against chemoresistant colorectal cancers: Inhibition of p38α modulates the effect of cisplatin in vitro and in vivo through the tumor suppressor FoxO3A. Cancer Lett. 344, 110–118.

Ghandi, M., Huang, F.W., Jané-Valbuena, J., Kryukov, G.V., Lo, C.C., McDonald III, E.R., Barretina, J., Gelfand, E.T., Bielski, C.M., Li, H., et al. (2019). Next-generation characterization of the Cancer Cell Line Encyclopedia. Nature 569, 503–508.

Iakoucheva, L.M., Radivojac, P., Brown, C.J., O'Connor,T.R., Sikes, J.G., Obradovic, Z., and Dunker, A.K. (2004). Intrinsic disorder and protein phosphorylation. Nucleic Acids Res. 32, 1037–1049.

Jassal, B., Matthews, L., Viteri, G., Gong, C., Lorente, P., Fabregat, A., Sidiropoulos, K., Cook, J., Gillespie, M., Haw, R., et al. (2020). The reactome pathway knowledgebase. Nucleic Acids Res. 48, D498–D503.

Knijnenburg, T.A., Wang, L., Zimmermann, M.T., Chambwe, N., Gao, G.F., Cherniack, A.D., Fan, H., Shen, H., Way, G.P., Greene CS, et al. (2018). Genomic and Molecular Landscape of DNA Damage Repair Deficiency across The Cancer Genome Atlas. Cell Rep. 23, 239–254.e6.

Nakatani Y., and Ogryzko, V. (2003). Immunoaffinity purification of mammalian protein complexes. Methods Enzymol. 370, 430–444.

Peserico, A., Germani, A., Sanese P., Barbosa, A.J., Di Virgilio V., Fittipaldi R., Fabini E., Bertucci C., Varchi G., Pat Moyer M., et al. (2015). A SMYD3 Small-Molecule Inhibitor Impairing Cancer Cell Growth. J. Cell. Physiol. 230, 2447–2460.

Proserpio, V., Fittipaldi, R, Ryall, J.G., Sartorelli, V., and Caretti, G. (2013). The methyltransferase SMYD3 mediates the recruitment of transcriptional cofactors at the myostatin and c-Met genes and regulates skeletal muscle atrophy. Genes Dev. 27, 1299–1312.

Rizzolo, P., Zelli, V., Valentina Silvestri, V., Virginia Valentini, V., Zanna, I., Bianchi, S., Masala, G., Spinelli, A.M., Tibiletti, M.G., Russo, A., et al. (2019). Insight into genetic susceptibility to male breast cancer by multigene panel testing: Results from a multicenter study in Italy. Int. J. Cancer. 145, 390–400.

Sander, C., Martens, J.W.M., and Lodewyk F. A. (2016). Wessels A novel independence test for somatic alterations in cancer shows that biology drives mutual exclusivity but chance explains most co-occurrence. Genome Biol. 17, 261.

Schneider, C.A., Rasband, W.S., and Eliceiri, K.W. NIH Image to ImageJ: 25 years of image analysis. (2012). Nat. Methods. 9, 671–675.

Silvestri, V., Zelli, V., Valentini, V. Rizzolo, P., Navazio, A.S., Coppa, A., Agata, S., Oliani, C., Barana, D., Castrignanò, T., et al. (2017). Whole-exome sequencing and targeted gene sequencing provide insights into the role of PALB2 as a male breast cancer susceptibility gene. Cancer 123, 210–218.

Tate, J.G., Bamford, S., Jubb, H.C., Sondka, Z., Beare D.M., Bindal, N., Boutselakis, H., Cole, C.G., Creatore, C., Dawson, E., et al. (2019). COSMIC: the Catalogue Of Somatic Mutations In Cancer. Nucleic Acids Res. 47, D941–D947.

Tian, S., Yan, H., Kalmbach, M., and Slager, S.L. (2016). Impact of post-alignment processing in variant discovery from whole exome data. BMC Bioinformatics. 17, 403.

Wang, L., Wang, S., and Li, W. (2012). RSeQC: quality control of RNA-seq experiments. Bioinformatics (Oxford, England). 28, 2184–2185.

Zannini, L., Lecis, D., Lisanti, S., Benetti, R., Buscemi, G., Schneider, C., and Delia D. (2003). Karyopherin-alpha2 protein interacts with Chk2 and contributes to its nuclear import. J. Biol. Chem. 278, 42346–42351.